Journal of Materials Chemistry C

ROYAL SOCIETY OF CHEMISTRY

REVIEW

View Article Online
View Journal | View Issue

Cite this: J. Mater. Chem. C, 2022, 10, 11105

Macromatrices for nanoscale particles

Xue Bai,[ab] Finn Purcell-Milton [b] and Yurii K. Gun'ko *[b]

Nanotechnology has been explored for several decades, and incredible advancements have been achieved across the field. This huge interest is due to nanomaterials exhibiting a range of unique properties, including the well-known quantum confinement effect that is observed in quantum dots (QDs). These nanoparticles (NPs) are generally prepared and stored in either aqueous or nonpolar solvents, with some of them being sensitive to oxygen, moisture and strong light which hinders their broad applications, in particular, for solid-state lighting and photovoltaics. The best strategy to mitigate these issues is to incorporate the NPs in airtight, moisture resistant, chemically, and thermally stable macromatrices to hold and protect them, rendering them far more suitable for applications. This review presents three main categories of macromatrices explored so far for NP encapsulating, including ionic macrocrystals, organic macrocrystals and polymeric materials. In addition, the corresponding preparation methods for each category of macromatrices and the recent progress in this area have been discussed in details. This review is expected to give the readers distinct insights into this emerging area.

Received 27th March 2022,
Accepted 29th June 2022

DOI: 10.1039/d2tc01244h

rsc.li/materials-c

1. Introduction

The talk entitled "There's Plenty of Room at the Bottom" delivered by Physics Nobel Laureate Richard Feynman in 1959 opened the gate to the new world – the world of nanoscale materials. Nanotechnology is the creation of functional materials, devices and systems through the control of matter on the nanometre length scale. When the dimension is within the 1–100 nm scale, materials reveal novel phenomena and properties, which can be exploited for brand new applications. The popularization of nanotechnology failed to take place until the arrival of sophisticated instrumentation. Later in the 1980s, the first scanning probe microscopy (SPM) was developed,[1] which was followed by the other well-known instrumentation, including transmission electron microscopy (TEM), scanning electron microscopy (SEM), energy-dispersive spectroscopy (EDX), atomic force microscopy (AFM), differential scanning calorimetry (DSC), X-ray diffraction (XRD) and so forth. All these state-of-art machines make the viewing and manipulating materials on the nanoscale come true. Ever since, various NPs have been synthesized and studied including but not limited to inorganic quantum dots (QDs) (traditional Cd-based QDs,[2–9] Cu-based QDs,[10–24] perovskite QDs,[25–36] carbon QDs,[37–40] graphene QDs[41–43] and Si QDs[44–46]) and metallic NPs (Au NPs[47–49] and Ag NPs[50–52]).

All the above NPs are prepared by either "top-down" processes using advanced lithographic, ablation, etching and sonicating techniques or "bottom-up" techniques based on the self-assembly of nanoscale species (with hot-injection, heating up, seeded growth methods and so forth being developed). The obtained NPs are normally stored in polar (water, ethanol and acetone) or nonpolar (toluene and chloroform) solvents based on the chemical nature of the NPs. The NP solution is suited for various characterization methods; however, they suffer from the low processability of their solutions for practical applications.

This issue can be tackled by embedding NPs into macromatrices. These matrices then allow easily processable phosphors to be used in a wide range of devices. To date, several categories of matrix materials have been explored for NP incorporation including: (1) inorganic macro-crystals, (2) organic macrocrystals, (3) polymeric materials and (4) other materials (clay, natural rubber and so forth). Embedding NPs into these macromatrices not only helps in improving their processability but also benefits their photostability and thermal stability. Encapsulating NPs into macromatrices helps in protecting the NPs from the external environment such as oxygen, moisture, heating, photon excitation and so forth that can easily induce the oxidation and degradation of the NPs. Incorporating NPs in suited macromatrices can preserve their original properties and make them more durable for a wide range of applications. Interestingly, to the best of our knowledge, there is only one perspective on ionic macrocrystals to seal QDs.[53] Otherwise, no

[a] Laboratory of Laser and Infrared Materials, CAS Key Laboratory of Materials for High Power Laser, Shanghai Institute of Optics and Fine Mechanics, CAS, Shanghai, China
[b] School of Chemistry and CRANN Institute, University of Dublin, Trinity College Dublin, Trinity College, College Green, Dublin D02, Ireland. E-mail: igounko@tcd.ie

other comprehensive review can be found covering this exciting field.

In this review, we aim to present the recent progress in this field, including the emerging materials best suited for incorporating NPs along with the developed loading techniques, and we believe that this review will inform researchers to choose the optimal materials to embed NPs for specific applications and further forward the advancement of this quickly evolving area by bringing a new wave of researchers.

2. Inorganic macrocrystals

Ionic macrocrystals are air- and moisture-tight, which means that they are one of the best candidates to embed and protect QDs for LED applications. Ionic macrocrystals have been widely investigated due to their outstanding performance with promising preparation methods being developed to date.

2.1 Formation of NP loaded inorganic macrocrystals

Inorganic macrocrystals are air- and moisture-tight, which means that they are one of the best candidates to embed and protect QDs for LED applications. A range of ionic salts such as NaCl, KCl, KBr, Borax, and LiCl have been employed as the macromatrix to incorporate QDs, and several methods have been developed to conduct the embedding process, including (1) slow evaporation promoted crystallization, (2) vacuum assisted crystallization, (3) liquid–liquid diffusion-assisted crystallization (LLDC), (4) the seed-mediated LLDC approach, and (5) the cold flow method.

As shown in Fig. 1A, the slow evaporation of the solvent is the traditional method to load QDs into soluble inorganic matrices. The basic mechanism behind this method is that the chosen salt crystallizes out of the solution, capturing QDs inside the crystal upon the slow evaporation of the solvent. In this method, the QDs need to be water soluble, which means that the QDs are either synthesized in an aqueous phase or have been transferred to the aqueous phase using ligand exchange or other phase transfer postsynthetic procedures. Under the slow evaporation rate of water, high quality, even a single crystal of the salt can be formed. Using the slow evaporation method, Kalytchuk *et al.* synthesized water-soluble CdHgTe QDs and incorporated the obtained QDs into a NaCl macromatrix for light-emitting devices.[54] It was performed by mixing the QD solution with a NaCl solution and allowing the water to evaporate slowly at 30 °C. The drawback of this method is that it is a time-consuming process (weeks). Since the crystallization time is quite prolonged, it is necessary to make sure that the QDs are stable in the aqueous phase to ensure the even distribution of QDs in the formed macrocrystals. In addition, if the QDs are made in a non-polar medium initially, a postsynthetic procedure such as ligand exchange or a phase transfer procedure has to be carried out then to make the QDs water soluble, which normally diminishes the photoluminescence quantum yields (PLQYs) of the QDs.

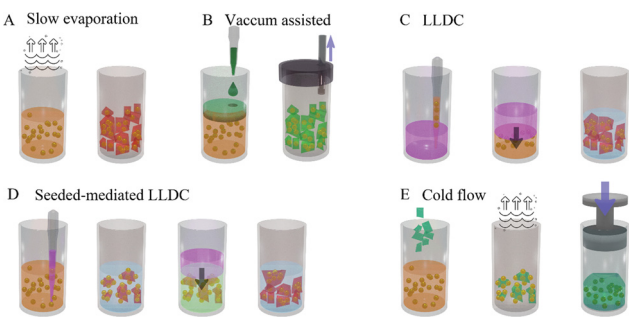

Fig. 1 Schematic illustration of the (A) slow solvent evaporation method, (B) vacuum-assisted method, (C) LLDC method, (D) seeded-mediated LLDC method and (E) cold flow method.

Compared to alkaline salts, borax has reduced ionic strength, which benefits the loading amount of QDs in the matrix. Marcus Adam *et al.* employed borax to replace NaCl using the same method to incorporate CdSe/ZnS QDs for LEDs,[55] resulting in a 3.4 time increase in QD loading in the obtained macromatrix compared to the NaCl matrix.

The vacuum-assisted process is based on the rapid evaporation of the solvent under a reduced pressure environment (Fig. 1B). Erdem *et al.* carried out the embedding of Cd-based QDs into LiCl powders using this method.[56,57] In their studies, LiCl solution in dry THF was prepared, and QDs were dispersed in dry THF after the evaporation of the original non-polar solvent. Then, the two obtained solutions were mixed and THF was evaporated quickly under vacuum resulting in fluorescent powders. Importantly, since the obtained colloidal QDs are relatively stable in THF and the drying process is very quick (around 2 h), it therefore is not necessary to transfer the QDs into the aqueous phase first.

As illustrated in Fig. 1C, the mechanism of the LLDC method is based on the solubility difference of the salt in two miscible solvents with different polarities. As exampled in Marcus Adam's work,[58] colloidal CdTe QDs were synthesized and transferred into the aqueous phase using a ligand exchange procedure. Following this, a aqueous saturated NaCl solution mixed with an aqueous QD solution. The obtained solution was injected slowly with a syringe beneath ethanol that was loaded into a vial. As the ethanol diffuses into the salt solution, the solubility of the NaCl decreases, which results in the co-crystallization of NaCl and QDs. Compared to the slow evaporation method, the advantages of LLDC is that it is less time consuming, and normally, the entire co-precipitation process takes 15–20 h under an ambient environment. Carbon QDs have also been successfully incorporated into the NaCl matrix using this method.[59] One problem with this technique is that the water soluble QDs are required which carries the same issues as discussed previously.

In order to solve this issue, the LLDC method has been modified to the seed-mediated approach that can be used to embed oil-soluble QDs directly by the same group. In the seed-mediated LLDC approach (Fig. 1D), the saturated NaCl solution in methanol is added to the dilute QD solution in chloroform, which results in the rapid crystallization of NaCl due to its much reduced solubility. Since this process occurs fast, the majority of QDs end up attached to the surface of the formed

NaCl small crystallites. These obtained seeds are used to repeat the LLDC procedure producing larger salt crystals with QDs sealed inside. In this case, the prior ligand exchange or phase transfer can be avoided.

The cold flow approach is based on the sintering behaviour of salts (KCl, KCl, NaCl, CsI, AgI, *etc.*) at high pressure, resulting in salt powder transforming into a transparent crystal at high pressure (Fig. 1E). Albrecht and his co-workers[60] demonstrated this technique for the first time to produce QD doped transparent crystals. In this method, the finely milled salt powder was mixed with the nonpolar solvent (chloroform or hexane) that was used to disperse oil-soluble QDs, and then the obtained dispersion solution of the salt was mixed with the oil-based QD solution. Then, the solvent was evaporated under reduced pressure on a rotary bath, which resulted in the QDs being deposited on the surface of the salt powder. After this, the dry sample underwent cold flow at 2.2 GPa pressure for 5 min, producing transparent salt pellets loaded with QDs. Using this technique, it took only several minutes to achieve a high loading of oil soluble QDs, a substantial step forward for this area. The summary of each method is listed in Table 1.

2.2 Properties of NP loaded inorganic macrocrystals

Based on the developed methods to embed QDs into ionic macromatrices, detailed studies have been carried out to investigate the effects of the ionic matrices on the properties of the incorporated QDs. In order to understand the difference among methods, Huang and his co-workers investigated the photostability of CdTe QDs embedded in the same NaCl matrix using three different methods,[65] comparing slow evaporation in water to methanol assisted LLDC and ethanol assisted LLDC methods. From this, it has been found that the CdTe QDs loaded *via* the slow evaporation and methanol assisted LLDC methods revealed higher photostability than that of the CdTe QDs sealed using the ethanol assisted LLDC method (Fig. 2A). It has been interpreted that the fast solidifying process of the ethanol LLDC method because of the lower solubility of NaCl in ethanol caused the incomplete encapsulation of QDs in NaCl, which induced fast oxidation to the QDs under continuous heating or high-energy photon-excitation. Some effort has been focused on the study of the influence of the ionic matrices on the optical properties of QDs. Müller *et al.* carried out detailed study on the enhanced optical properties of Cd-based QDs embedded in an ionic matrix.[66] In their work, CdTe QDs have been loaded into a NaCl matrix using the slow evaporation method, which gave a much increased PLQY from 50% to 80%. The reason for the enhanced PLQY of the embedded CdTe QDs is attributed to the curing of surface defects through the formation of a thin passivation layer of $CdCl_x$ most likely (Fig. 2B), since such an increase of the PLQY has not been observed when studying CdTe/ZnS core/shell QDs loaded into a NaCl matrix and when the CdTe QDs were loaded into a borax matrix. Later, Okrepka *et al.* used the interband quantum transition theory to explain the detected red shift of CdTe QDs after encapsulated into the KBr ionic matrix.[67] The reason can be attributed to the decrease in the height of potential barriers when the external environment changed from water to KBr.

The encapsulation of QDs in ionic macrosalt crystals makes them more than suited for solid-state lighting applications. As shown in Fig. 2C, Otto *et al.* synthesized CdTe QDs in an aqueous system and packaged the obtained QDs into several different ionic matrices (NaCl, KCl, KBr, *etc.*) using the traditional slow evaporation method for LEDs.[61] Normally, the QDs need to be fixed in a silicone matrix for the hybridization of the color converter on the LED platform, which would cause a detrimental influence on the optical properties of the QDs. After the QDs have been incorporated into the ionic matrices, no degradation to the PL of the QDs has been observed upon being fixed within the silicone matrix, which demonstrates the excellent protection afforded by the ionic matrices to QDs. Not only Cd-based QDs, but recently researchers have also started attempting to incorporate Cu-based QDs into various ionic matrices. CIZS/ZnS core/shell heterostructured QDs were incorporated into 2 different – LiCl and borax – matrices using 2 different methods (vacuum assisted and slow evaporation, respectively.).[63] In their work, as a proof of concept, a colour conversion LED has been fabricated with the QD-in-LiCl solid composite.

In summary, incorporating QDs into air- and moisture-tight ionic macrocrystals not only helps in improving the processability of QDs, but also protects the QDs from the external environment and enhances their photostability, thermal stability and chemical stability, even demonstrating the enhanced PLQYs of Cd-based QDs. These factors illustrate the promising future of QDs for solid-state lighting applications.

3. Organic macrocrystals

Aside from inorganic salt macro-crystals, there exists another category – organic macrocrystals – being explored recently. Unlike the inorganic salts, organic macromaterials including sucrose and anthracene lack the ionic strength, which renders

Table 1 Summary of methods that are commonly employed to incorporate QDs into ionic macromatrices

Method	Slow evaporation	Vacuum assisted	LLDC	Seed-mediated LLDC	Cold flow
QDs	Water-soluble	Oil-soluble	Water-soluble	Oil-soluble	Oil-soluble
Salts	Alkaline borax	LiCl	Alkaline	Alkaline	Most alkaline
Solvent	Polar (normally water)	Nonpolar	Polar	Nonpolar and polar	Nonpolar
Time (variable)	1–4 weeks	2 h	15–20 h	15–20 h	5 min
Advantage	High quality macrocrystals	Less time consuming	Less time consuming	No prior phase transfer	High loading of QDs
Reference	61,62	63	64	58	60

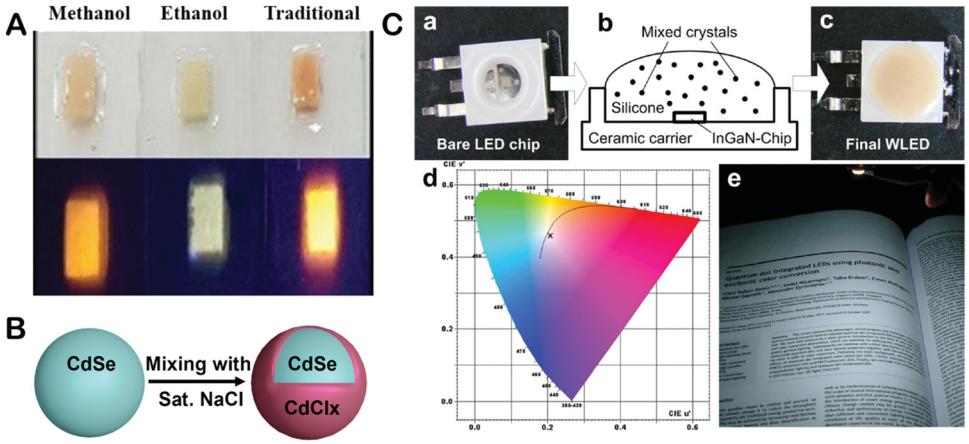

Fig. 2 (A) CQD + NaCl for three synthesis methods under ultra-violet (UV) light. Reproduced with permission from ref. 65, Copyright 2019, MDPI. (B) Schematic shows the proposed mechanism for the observed increased PLQY of the CdTe QDs after being incorporated in the NaCl matrix[66]. (C) The LED that was built with the obtained macrocrystals: bare blue emitting 1 W InGaN LED chip (a), schematics of its hybridization with mixed crystals embedded in silicone (b), and the resulting white LED (c). Colour coordinates of the WLED are shown as a cross in the CIE 1976 diagram (d). The colour temperature of the device as derived from the nearest point in the Planckian locus is around 6500 K. A title page reprinted with permission from ref. 15 illuminated by the WLED (e). Reproduced with permission from ref. 61. Copyright 2012, ACS.

this type of macro-crystal ideal for a range of specific NPs, for example metal NPs which aggregate severely in ionic solutions.

3.1 Sucrose macrocrystals

Sucrose is one of the most common ingredients used in kitchens, while, in 2014, sucrose was employed for the very first time by Erdem *et al.* to encapsulate Au NPs producing "Sweet plasmonic crystals".[68] Sucrose was chosen on purpose to avoid the aggregation of Au NPs in solution (ions strongly induce the aggregation of metal NPs in the salt solution). The growth of the sucrose macrocrystals was based on the slow evaporation of an aqueous sucrose solution for approximately 10 days. The plasmonic nature of Au NPs has been preserved after being embedded into these sucrose macrocrystals, clearly shown by the increase of the fluorescence of CdTe QDs from 24% to 38% after loading into the sucrose macrocrystals along with Au NPs. The enhanced emission was due to plasmonic coupling between the CdTe QDs and the Au NPs. Later, all-organic monoliths have been achieved by incorporating oligomer NPs into sucrose macrocrystals.[69] The PLQYs and temperature stability of oligomer NPs are not high enough to employ them for any practical applications. In order to explore this area, the authors sealed the obtained oligomer NPs in sucrose macrocrystals using the slow evaporation method at RT. As shown in Fig. 3, it has been revealed that the PLQY of the oligomer NPs enhanced from 3.4% of the NP dispersion solution to 43.5% of the obtained macrocrystals. The reason for the increased PLQY was attributed to the reversible physical and/or possibly noncovalent interactions between the oligomer NPs and the sucrose matrix. In addition, the 3-fold improved temperature stability was realized for this all-organic system. Following this, the obtained macrocrystals were demonstrated as colour converters on a blue LED chip successfully. Considering the low cost of the material and the simplicity of the preparation method, along with the robustness of the macrocrystals, sucrose demonstrates a promising future for incorporating a broader range of NPs for solid-state lighting applications.

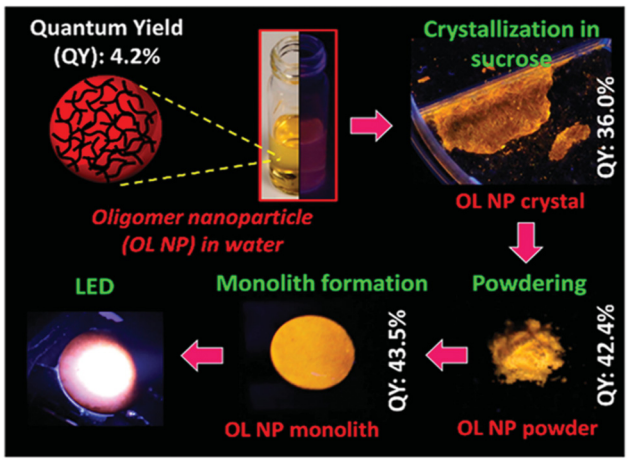

Fig. 3 Schematic illustrates the building process of the LED chip starting from the oligomer NP solution to sucrose macrocrystals. Reproduced with permission from ref. 69. Copyright 2016, ACS.

3.2 Anthracene macrocrystals

Another organic macrocrystal that has been extensively explored is anthracene ($C_{14}H_{10}$), an organic molecule composed of benzene groups with a wide optical band gap. Unlike sucrose which is soluble in water, anthracene is soluble in nonpolar solvents such as toluene and chloroform. Therefore, the non-polar nature of anthracene offers significant benefits to the formation of NP macrocrystals since no prior ligand exchange or phase transfer is needed for the use of high-quality NPs prepared in non-polar solvents. In 2015, CdSe/CdZnSeS/ZnS alloyed QDs for the first time were encapsulated into organic host macrocrystals of anthracene using a slow solvent evaporation method.[70,71] Due

to the overlap between the absorption spectrum of the QDs and the emission peaks of the host crystals, nonradiative energy transfer (NRET) between the donor (anthracene) and the acceptor (QDs) has been investigated and polarized emission from the QDs has been detected. In addition, interestingly, the presence of the QDs leads to the formation of larger macrocrystals of over 1 cm in one dimension. Without the inclusion of QDs, the size of the crystals was of subcentimetre size. Apparently, the introduced NPs play an important role in the growth of the macrocrystals. A detailed study of the effects of Fe_3O_4 NPs on anthracene single crystals has also been performed.[72] In this work, pure anthracene macrocrystals and Fe_3O_4 NPs – doped anthracene macrocrystals were prepared using the slow solvent evaporation method at RT with chloroform as the solvent. It was revealed that the emission intensity of crystals in the blue region increased, the conductivity was enhanced, and the decomposition temperature was decreased by 4 °C from the melting point of the pure anthracene crystal due to the doping of Fe_3O_4 NPs. And, they have successfully embedded other metal oxides (ZnO and TiO_2) into anthracene macrocrystals.[73] In 2018, Shen *et al.* reported a novel one-step method to prepare perovskite QDs ($CsPb(Br/I)_3$)–anthracene composites for white LEDs.[74] Instead of using the traditional slow solvent evaporation method, anthracene was added during the synthesis of the perovskite QDs, which was performed by mixing anthracene with lead salts in octadecene, oleylamine and oleic acid to make the precursor solution followed by the swift injection of the cesium precursor solution. The experimental results revealed the even distribution of the perovskite QDs in anthracene crystals. NRET has been found between the perovskite QDs (acceptor) and the host crystals (donor). The quenching temperature of the QDs has been enhanced from 50 °C for pure QDs to 100 °C for the composites. Finally, highly efficient white light-emitting devices have been built with the obtained composites as shown in Fig. 4.

4. Polymeric matrices

Polymeric materials have been explored as the macromatrix to incorporate QDs, in particular, for photovoltaic applications, such as solar cells and solar concentrators. Polymers such as PMMA, PS, POSS, thiol–ene polymers, thiol–yne polymers and some copolymers have been investigated to date. Among the wide range of polymeric materials, PMMA turns out to be the most commonly employed one as the matrix to embed NPs due to its transmittance from the near UV region to the NIR (near infra-red) region of the spectrum, nontoxicity, good mechanical properties, high thermal stability and excellent moisture resistance. There are several ways to embed the QDs into these polymeric matrices, including (1) solution casting, (2) spin coating, (3) one-step polymerization and (4) two-step polymerization procedures.

4.1 Solution casting of PMMA

The solution casting method is based upon the mixing of the NPs and PMMA solution in non-polar solvents (DMF, toluene, chloroform and so forth). This solution is cast into a mould followed by drying of the solvent, resulting in the formation of PMMA films loaded with the corresponding NPs. CdSe QDs have been sealed into a thin PMMA film using this method, and

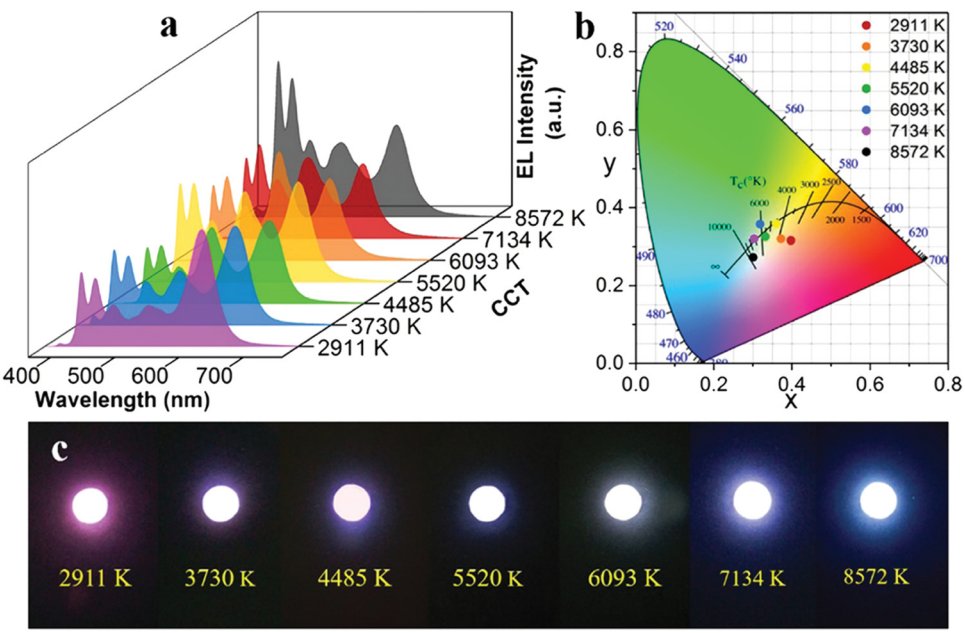

Fig. 4 The WLED work that is based on the perovskite QDs ($CsPb(Br/I)_3$)–anthracene composites: (a) EL spectra of UV LED chips coated with a mixture of green light-emitting $CsPb(Br_{0.8}I_{0.2})_3$@anthracene and red light emitting $CsPb(Br_{0.4}I_{0.6})_3$@anthracene composite powder with various mass ratios. (b) CIE 1931 colour coordinates of WLED devices A–G. (c) True-colour images of WLED devices A–G. Reproduced with permission from ref. 74. Copyright 2018, ACS.

then the fluorescence, thermal and mechanical properties of the resultant samples have been studied.[75] It has been found that, upon the loading of the QDs, the hardness of the thin PMMA film has been enhanced, along with the increase of T_g (glass transition temperature) from 113.41 to 115.22 °C. At the same time, the fluorescence of the QDs has been preserved and the PL lifetime prolonged from 1.8 ns to 2.1 ns. A small blue shift from 610 nm of the QD parental solution to 606 nm of the composite was attributed to the minor aggregation of the QDs during the preparation process. There are a number of other reports of encapsulating NPs in a PMMA matrix using this method.[76]

4.2 Spin coating of PMMA

Spin coating is a straightforward method that is similar to solution casting. By mixing the solution of NPs and the solution of PMMA, the solution is spin-coated onto certain substrates. In 2011, CdSe QDs and CdTe QDs were sealed in a PMMA matrix using this method using toluene as the solvent, and for the very first time, wave guiding of the fluorescence from the QDs in the PMMA matrix was observed.[77] All inorganic perovskite QDs $CsPbX_3$ (X = Cl, Br, and I) tend to decompose when exposed to moisture, heat or strong photo radiation due to their ionic nature. Zhang *et al.* synthesized all inorganic perovskite QDs using a hot-injection method and included the obtained QDs into the PMMA matrix using the spin coating method, using chloroform as the solvent and PET as the substrate.[78]

4.3 Polymerization of MMA

The main limit of solvent casting and spin coating methods is that the thickness of the obtained composite films is only possible up to several micrometres, with the issues regarding excessive shrinkage of the composite when drying. In addition, the solvent evaporation process needs to be under careful control to prevent the formation of air bubbles, which affects the quality of the obtained composite films to a substantial level. Under this situation, *in situ* loading of the NPs into the polymeric matrices through the polymerization procedure has been proposed, including one-step and two-step polymerization being used to prepare NP–polymer composites.

One-step polymerization is performed by mixing the NPs, the monomer, and the initiator and/or cross-linker, which is followed by heat-induced polymerization or UV light-initiated polymerization. Fig. 5A and B show the PMMA polymer blocks loaded with perovskite QDs and ZnO QDs, prepared *via* the one-step polymerization procedure. Protesescu *et al.* synthesized highly emissive cesium lead halide QDs and embedded the obtained QDs into a PMMA matrix successfully using both heat-induced polymerization (thermal radical initiator) and UV curing (photoinitiator).[79] Jinku Xu and Dongmei Li expanded on the one-step polymerization method utilizing an MMA monomer and polymerizable group-capped ZnS QDs. Using this novel approach, outstanding loading of ZnS QDs was achieved reaching as high as 41wt%.[80]

The one-step polymerization is a method that achieves the preparation of high-quality large-scale polymer blocks.

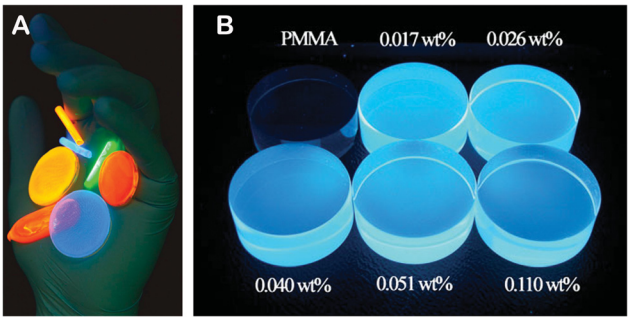

Fig. 5 (A) PMMA polymer blocks loaded with $CsPbX_3$ QDs prepared using the one-step polymerization method. Reproduced with permission from ref. 79, Copyright 2015, ACS. (B) ZnO QD–PMMA monoliths prepared using the one-step polymerization technique. Reproduced with permission from ref. 84, Copyright 2007 Wiley.

However, one issue with this method is that the direct contact of the QDs with the harsh initiators causes diminished PLQYs of the QDs,[81,82] which is one of the main factors for the limited efficiency of the corresponding devices. The two-step polymerization method has been proposed to minimize the interaction between the QDs and the initiator and preserves the optical properties of the embedded QDs.[83] In their work, a "syrup" was prepared in the first step, which was performed by mixing the purified MMA monomer and the initiator AIBN and heating to 80 °C to start the pre-polymerization. The formed "syrup" was quenched at the onset of vigorous boiling. In the second step, the mixture of QDs, MMA monomer and lauryl peroxide was introduced into the "syrup", followed by transferring the viscous solution into a casting mould for the polymerization to take place. Using this method, the optical properties of giant CdSe/CdS QDs have been preserved. Finally, luminescent solar concentrators with an optical efficiency of $>10\%$ and an effective concentration factor of 4.4 were demonstrated.

4.4 NP–PMMA composite properties

With the above developed encapsulating techniques, there are plenty of important studies in this area, including the works to study the distribution details of the NPs in the polymeric material and investigate the effects of the loaded NPs on the properties of the PMMA matrix. Patidar *et al.* incorporated CdS QDs in a PMMA matrix using the solution casting method and employed TEM and small angle X-ray scattering (SAXS) to reveal the size and shape of the QDs after loading in PMMA.[96] In their work, 2, 4, 6 and 8 wt% of QD loading has been tested with the SAXS results demonstrating that the composites of up to 6 wt% contained isolated QDs and a narrow size distribution; for the 8 wt% sample, it showed the tendency of agglomerate formation, which was consistent with the observation from TEM images. It has also been found that, upon the loading of the CdSe QDs, both the storage modulus and T_g of the PMMA matrix have been enhanced. On the other hand, the polymeric matrices also influence the properties of the encapsulated NPs. Moura *et al.* incorporated a fixed amount of CdTe QDs (2 wt%) into a broad range of polymeric materials using the solution casting

Table 2 Summary of the recent studies on NPs embedded in PMMA

Material	NPs	Method	Initiator/solvent	Device	Ref.
MMA	CdSe/CdS/CdS/$Cd_{0.75}Zn_{0.25}S$/ $Cd_{0.5}Zn_{0.5}S$/$Cd_{0.25}$ $Zn_{0.75}S$/ ZnS/ZnS QDs	One-step photopolymerization	2,4,6-Trimethylbenzoyldiphenylphosphine oxide (TPO)	—	82
MMA	ZnO QDs	One-step heat-induced polymerization	AIBN	—	84
MMA	$CuInS_2$/ZnS QDs	One-step heat-induced polymerization	AIBN	LSCs	85
PMMA	InP/ZnS QDs MWCNTs	Spin coating	THF	—	86
PMMA	CdS QDs	Solution casting	Chloroform, ethanol, benzoyl peroxide	—	87
PMMA	In_2O_3 NPs	Solution casting	Chloroform	—	88
MMA	CdS QDs	One-step heat induced polymerization	Benzoyl peroxide	—	89
MMA	CdTe QDs	One-step heat induced polymerization	Benzoyl peroxide	—	90
MMA	Si QDs	One-step heat induced polymerization	AIBN	LSCs	91
MMA	Si QDs	One-step heat induced polymerization	AIBN	LSCs	92
PMMA	CdS QDs, CdTe QDs, CdSe QDs	Spin coating	toluene	Waveguides	93
PMMA	CdS QDs, CdTe QDs, CdSe QDs	Spin coating	Toluene	Waveguiding	94
MMA	SiO_2, ZnO, TiO_2 NPs	One-step heat induced polymerization	AIBN	LSCs	95

method.[97] After being sealed in the polymeric matrix, a slight increase of the size of QDs has been revealed based on the TEM images. In addition, a slight red shift of the emission peak of the QDs can be observed, and it was attributed to the increased size of the QDs and the agglomerates that formed in the matrices. The above reports demonstrated that the presence of NPs affects the thermal and mechanical properties of the polymeric host materials, and at the same time, the alteration of the optical properties and/or even the size of the NPs can be observed after being encapsulated in the polymeric blocks. To date, there have been many more studies on the embedding of NPs into the PMMA matrix, and the information is summarized in Table 2.

4.5 Other NP–polymer composites

Besides the commonly used PMMA block, there are also some other polymeric materials that are under extensive investigation, including the off-stoichiometric thiol–ene (OSTE) polymer and the off-stoichiometric thiol–yne (OSTY) polymer. They are both nontoxic and non-sensitive to oxygen and low-polymerization shrinkage polymeric materials. The reaction between both thiol and alkene and alkyne belongs to the "click" family. Polymerization proceeds *via* a rapid step-growth, free-radical chain process. In addition, a wide range of NPs can be embedded into OSTE and OSTY polymers, such as Au NPs and QDs.

Alkyl-terminated Si QDs have been encapsulated in the OSTE matrix, using 10 seconds of photopolymerization of the mixture of the QDs, allyl monomers, thiol monomers and the photoinitiator Irgacure-184.[98] In this work, a strong enhancement of the PLQY of the embedded Si QDs has been revealed and was attributed to the passivation effect of the OSTE radicals on the dangling bonds on the QD surface (Fig. 6A).

In another study,[99] $CdSe/Cd_{1-x}Zn_xSe_{1-y}S_y$ QDs capped with short ligands with simple alkane backbones have been incorporated in the OSTE block using thiol–ene chemistry. It has been found that very short ligands produced a substantial increase in QD loading (up to 30% compared to generally 1% or even less).[99]

In 2018, Stewart *et al.* synthesized novel ligands to functionalize CdSe/ZnS QDs and encapsulated the functionalized QDs

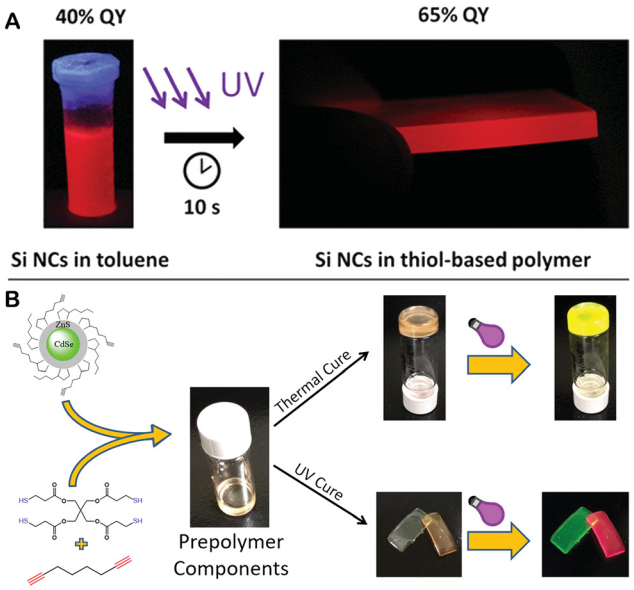

Fig. 6 (A) Photopolymerization used to incorporate Si NPs in the OSTE polymer block. Reproduced with permission from ref. 98. Copyright 2017, ACS. (B) Schematic illustrates the method to embed CdSe/ZnS QDs into the OSTY polymer block using either thermal polymerization or photopolymerization. Reproduced with permission from ref. 100. Copyright 2018, ACS.

into the OSTY polymer block.[100] As illustrated in Fig. 6B, both reactive dihydrolipoic acid (DHLA)–alkyne and an inert DHLA–butyl ligand have been synthesized to functionalize the as-synthesized CdSe/ZnS QDs *via* ligand exchange. Both ligands are based on dithiol groups, which means that the two ligands have higher affinity to QDs than monothiol-based ligands, meaning that ligand desorption can be minimized during any further procedure. The reactive ligands benefit the active participation of the QDs during polymerization, while the inert ligands ensure the stability of the QDs in the polymerization system. Then the functionalized QDs were incorporated into OSTY blocks using either a thermal curing or a photopolymerization method with optical properties being preserved.

Surface-enhanced Raman spectroscopy (SERS) active films and fibres have been obtained by encapsulating Au NPs functionalized

with thiophenol (has well studied SERS signatures) in OSTY polymers by Boyd *et al.*[101] The SERS response was detected that was proportional to the aggregation of the Au NPs sealed in the matrix and the amount of thiophenol present. A relatively time-consuming procedure (3 weeks) has been proposed to ensure the even distribution of Au NPs being incorporated in the OSTE block.[102] The work started with the precomplexation of Au NPs and the thiol, which was performed by stirring the mixture of Au NPs and thiol for weeks. Then, the triene along with the photoinitiator Irgacure 651 was added into the mixture of Au NPs and thiol, which was followed by the photocuring process.

Besides the straightforward incorporation of NPs in OSTE and OSTY polymers, more delicate micropatterned QD–polymer composites were reported using the thiol–ene reaction and imprinting lithography techniques.[103] In this work, three kinds of CdSe/ZnS QDs were employed (neutral QDs, positive QDs and positive QDs containing allylic groups) and it was claimed that the synergetic effect of the repulsion among the positive QDs and the chemical binding between the surface of the QDs and the matrix achieved the uniform dispersion of the QDs in the matrix, ensuring that a robust composite was obtained.

The above discussed polymeric materials including PMMA, OSTE and OSTY are mostly utilised as matrices to incorporate NPs, and there are also some other polymers that are under investigation. For example, PLMA and the newly introduced copolymer PSt-*b*-PIB-*b*-PSt (poly(styrene-*block*-isobutylene-block-styrene)). The one-step polymerization method was also used to incorporate Cu-based CISeS/ZnS QDs in the PLMA polymer, which was performed by adding the photoinitiator (IRGACURE 651) and the crosslinker (EGDM) into the mixture of the QDs and the LMA monomer. UV light (365 nm) was employed to initiate polymerization producing large area, high-quality luminescent solar concentrators with an optical power conversion efficiency of up to 3.27%.[104] In another study, the encapsulation of CdSe NPLs (nanoplatelets) and PbS QDs was performed in the copolymer PSt-*b*-PIB-*b*-PSt by employing the drop casting method.[105] In this work, it has been found that the stabilities of the nanoparticles-in-PIB and -PSt-*b*-PIB-*b*-PSt composites were even higher than that of NPLs (QDs)-in-PLMA, which indicates the promising prospect of isobutylene-based polymers as the matrix to incorporate QDs for solid-state lighting and photovoltaic applications.

4.6 Applications based on NP loaded polymeric matrices

Encapsulation technology is very helpful for a range of practical applications. Polymeric matrices that host NPs have a wide range of applications such as nonlinear optical devices, displays, solar cells, light emissions, *etc.* In this section, we take nonlinear optical devices and LEDs as examples, to make a summary of the applications of NP loaded matrices.

Nonlinear optics is the study of the behaviour of light in nonlinear materials. When the light transverses in the nonlinear media, the polarization density is nonlinear to the electric field of the light.[106–108] For example, saturable absorption is an interesting nonlinear optical behaviour in which the transmission increases as the intensity of the incident light increases.[109–112] Two photon absorption is another important nonlinear optical phenomenon, in which an electron jumps from ground states to excited states by simultaneously absorbing two photons, resulting in the transmission decrease as the density of the incident light increases.[113] These nonlinear optical phenomena have been observed in many NPs. However, most of these NPs are obtained in solutions and therefore cannot be directly employed as a device for nonlinear optical applications. To have a better application of these NPs, many polymeric matrices such as PMMA have been used to package the NPs for nonlinear optical applications. Black phosphorus quantum dots (BPQDs), for instance, were produced using small molecule-assisted liquid-phase exfoliations and their dispersions were proved by the open-aperture Z-scan to have strong saturable absorption from the visible region to the near infrared region.[114] BPQDs were employed to fabricate the BPQD/PMMA composite nanofiber film, which can be used as a photonic device for mode-locking.[115] By incorporating this device into the cavity of an erbium-doped fiber (EDF) laser, picosecond laser pulses were generated at a central wavelength of 1567.6 nm.[115] Another similar example is to place CdSe QD loaded PMMA into the cavity of the ytterbium-doped fiber laser (YDFL), producing Q-switched and mode-locked fiber lasers with power outputs of 110 mW and 280 mW, respectively.[116]

Quantum dot loaded polymeric matrices with different structures have been widely utilized for light-emitting applications. A typical configuration is to mix the quantum dots with polymeric matrices to fabricate solid composite structures. W. Chung *et al.* prepared the mixtures of CdSe QDs and PMMA as phosphors to cover an InGaN 460 nm blue emission LED chip, which can obtain an emission of the white light.[117] A simple composite structure is to cover the QD layer with the polymetric matrix layer directly. In 2014, X. Dai *et al.* fabricated a LED using CdSe–CdS core–shell QDs as the emitter covered by the PMMA layer, which is the key component of the device.[118] They obtained a colour-saturated deep-red emission with high external quantum efficiencies of up to 20.5% and a long lifetime of more than 100 000 hours at 100 cd m^{-2}.[118] Another interesting configuration is the sandwich structure with PMMA and QD multilayers. A sandwich structure with two PMMA layers that were inserted into a pair of CdSe/ZnS QD layers respectively was used as the active layer of a LED.[119] This LED had obtained a luminance of 194 038 cd m^{-2} and a high current efficiency of 17.8 cd A^{-1}.[119]

In addition, NP loaded polymeric matrices have a lot of applications in other fields, such as solar concentrators[83,120] and displays,[121] in which polymeric matrices act as the bridge between the NPs and the practical applications.

5. Other matrices

Except for the three main categories, several unusual matrices attract research attention and are being used to embed NCs for certain applications successfully, for example silkworm silk, natural rubber, clay and glasses.

An electrostatic absorption method was used to embed the CdTe QDs with green, yellow, red and NIR fluorescence using poly(diallyldimethylammonium chloride) as the fixer, producing fluorescent silk.[122] It has been found that the fluorescent silk was stable in neutral and alkaline solutions with no QDs being released. Meanwhile, the fluorescence of the silk decreased significantly in acidic solutions. It was believed that the obtained fluorescent silk is promising for fabricating fluorescent cloth and anticounterfeiting labels. In this work, MPA-coated water soluble CdTe QDs were used, which means that MPA coated Cu-based counterparts could be used to replace the toxic Cd-based QDs in future work.

Natural rubber is a renewable polymer and consists of poly-1,4-cisisoprene linked units that can be obtained from trees.[123,124] Natural rubber has a high solubility in water which renders it the polymeric material to embed aqueous soluble NPs. As shown in Fig. 7 top, MSA coated water soluble CdTe QDs were sealed in the flexible natural rubber using the solution casting method, which was performed by mixing the natural rubber aqueous solution and the QD solution and the mixture was deposited on the glass slide and dried at RT.[125] It has been found that the presence of QDs did not affect the mechanical and thermal properties of the natural rubber host, and the optical properties of the sealed QDs have been preserved. Since most of the polymeric materials are used to incorporate oil–soluble NPs, water soluble natural rubber would be an excellent candidate to encapsulate and protect NPs prepared in the aqueous phase.

Silicate salt clay is cheap, commercially available and can be dispersed well in the aqueous phase. To date, water soluble MPA capped CdSe/ZnS QDs and water–soluble Si NPs have been embedded in a clay host based on the charge–charge interaction between the surface of QDs or the NPs and clay plates, which was performed using the solution casting method[126,127] (Fig. 7 bottom). It has been claimed that the large surface area of clay–polymer films can be easily made by solution casting a mixture of clay aqueous solution and an aqueous solution of a water–soluble polymer.[128] For example, the Si NP/clay/PVA film was prepared using the preformed composite of Si NPs and clay.[126] The ease of clay to be incorporated into large area free standing water–soluble polymeric matrices makes this fluorescent system very promising for solid-state lighting applications.

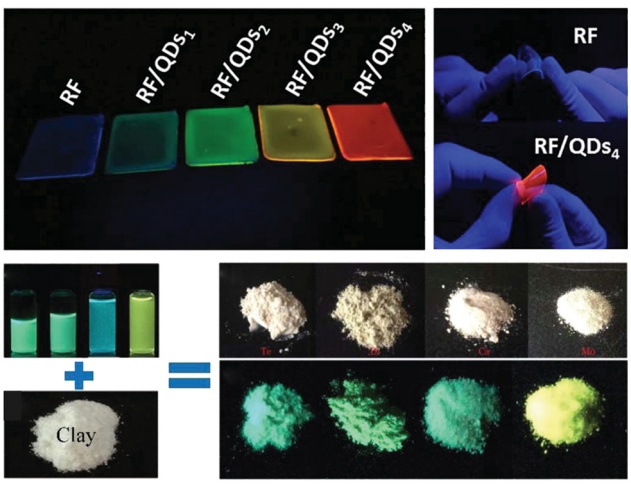

Fig. 7 Top: The pictures of the pure rubber film and the rubber films with CdTe QDs incorporated. Reproduced with permission from ref. 125. Copyright 2017, Wiley. Bottom: The pictures demonstrate the obtained Si NPs sealed in clay. Reproduced with permission from ref. 126, Copyright 2018, RSC.

Inorganic glasses are important inorganic matrices for embedding NPs due to their large damage threshold and high mechanical and chemical stabilities.[129] Many methods to prepare NP/glass composites have been developed such as the traditional melting-quenching method,[130] the ion-exchange method,[131,132] the sol–gel method[133,134] and the ion-implantation method.[135,136] To date, a variety of QDs including Cd-based QDs, Pb-based QDs and perovskite QDs have been embedded into glass matrices successfully.[137–140] The QD embedded glasses have a wide range of applications such as LEDs,[141] optical filters,[142,143] solar concentrators for windows,[144] nonlinear optics[145,146] and so forth. Hence, glasses are an excellent host for embedding NPs.

6. Conclusions and future outlook

In this review, we have summarized the most commonly employed macromatrices for NPs, including the most recent development, the developed techniques for corresponding materials and the practical solid-state lighting and photovoltaic applications based on the successful incorporation of NPs into these matrices, including ionic macrocrystals, organic macrocrystals, polymeric matrices and other emerging materials. The methods and techniques that have been developed to encapsulate NPs in each type of material have been explained in detail along with the studies to modify and improve the existing methods. A series of methods have been developed to incorporate both aqueous soluble NPs and oil–soluble NPs in various matrices with much minimized aggregation of the NPs and much minimized effects on the original properties of the NPs. In addition, many studies explore the applications of these composites in solid-state lighting and photovoltaic use cases.

Incorporating NPs, with outstanding properties, paves the way for nanotechnology to revolutionize a range of applications. Though a number of noteworthy results have already been achieved, this area is still in its early stage. Currently, most of the studies are based on Cd-based QDs with isotropic spherical morphologies. Meanwhile, presently due to the fast development of NP synthetic techniques, highly fluorescent Cu-based QDs with isotropic and anisotropic shapes are available for example.[24] For practical applications, Cu-based nanostructures are a very promising candidate to replace Cd-based ones due to their high quality, nontoxicity, much longer emission lifetimes and other specific advantages.[23,147] In addition, quantum confined nanocrystals with anisotropic morphologies for example nanorods and nanoplatelets display polarized emission;[148] if these structures can be aligned in a polymeric matrix, they would be ideal for photovoltaic applications,[149] a possibility deserving of more attention. Another issue is the low loading levels of NPs

that can be embedded into the matrices, normally only achieving less than 1 wt%, which greatly limits their use cases. More effort can be devoted to mitigating these issues and making the best use of NP loaded composites.

Author contributions

Xue Bai drafted the original manuscript. Finn Purcell-Milton and Yurii K. Gun'ko checked and edited the final manuscript.

Funding sources

This research was funded by the China Scholarship Council (CSC), Science Foundation Ireland and Biorbic, Bioeconomy Research Centre (grant number SFI 16/RC/3889) for financial support.

Conflicts of interest

There are no conflicts to declare.

Acknowledgements

The authors would like to thank the China Scholarship Council (CSC), Science Foundation Ireland and Biorbic, Bioeconomy Research Centre (grant number SFI 16/RC/3889) for financial support.

References

1 D. M. Eigler and E. K. Schweizer, Positioning single atoms with a scanning tunneling microscope, *Nature*, 1990, **344**(6266), 524–526.
2 J. Cheng, *et al.*, Optically Active CdSe-Dot/CdS-Rod Nanocrystals with Induced Chirality and Circularly Polarized Luminescence, *ACS Nano*, 2018, **12**(6), 5341–5350.
3 S. Ithurria, G. Bousquet and B. Dubertret, Continuous transition from 3D to 1D confinement observed during the formation of CdSe nanoplatelets, *J. Am. Chem. Soc.*, 2011, **133**(9), 3070–3077.
4 N. Mishra, *et al.*, Continuous Shape Tuning of Nanotetrapods: Toward Shape-Mediated Self-Assembly, *Chem. Mater.*, 2016, **28**(4), 1187–1195.
5 A. Sitt, *et al.*, Highly emissive nano rod-in-rod heterostructures with strong linear polarization, *Nano Lett.*, 2011, **11**(5), 2054–2060.
6 K. Wu, *et al.*, Efficient Extraction of Trapped Holes from Colloidal CdS Nanorods, *J. Am. Chem. Soc.*, 2015, **137**(32), 10224–10230.
7 J. Zhou, *et al.*, A Two-Step Synthetic Strategy toward Monodisperse Colloidal CdSe and CdSe/CdS Core/Shell Nanocrystals, *J. Am. Chem. Soc.*, 2016, **138**(20), 6475–6483.
8 J. Chang and E. R. Waclawik, Controlled synthesis of $CuInS_2$, Cu_2SnS_3 and Cu_2ZnSnS_4 nano-structures: insight into the universal phase-selectivity mechanism, *CrystEngComm*, 2013, **15**(28), 5612–5619.
9 B. Kim, *et al.*, $CuInS_2$/CdS-Heterostructured Nanotetrapods by Seeded Growth and Their Photovoltaic Properties, *ACS Appl. Nano Mater.*, 2018, **1**(6), 2449–2454.
10 E. Cassette, *et al.*, Synthesis and Characterization of Near-Infrared Cu–In–Se/ZnS Core/Shell Quantum Dots for In vivo Imaging, *Chem. Mater.*, 2010, **22**(22), 6117–6124.
11 J. Park, *et al.*, CuInSe/ZnS core/shell NIR quantum dots for biomedical imaging, *Small*, 2011, **7**(22), 3148–3152.
12 B. Chen, *et al.*, Highly Emissive and Color-Tunable $CuInS_2$-Based Colloidal Semiconductor Nanocrystals: Off-Stoichiometry Effects and Improved Electroluminescence Performance, *Adv. Funct. Mater.*, 2012, **22**(10), 2081–2088.
13 P. H. Chuang, C. C. Lin and R. S. Liu, Emission-tunable $CuInS_2$/ZnS quantum dots: structure, optical properties, and application in white light-emitting diodes with high color rendering index, *ACS Appl. Mater. Interfaces*, 2014, **6**(17), 15379–15387.
14 M. Gromova, *et al.*, Growth Mechanism and Surface State of $CuInS_2$ Nanocrystals Synthesized with Dodecanethiol, *J. Am. Chem. Soc.*, 2017, **139**(44), 15748–15759.
15 Y. Kim, *et al.*, Controlled Synthesis of $CuInS_2$/ZnS Nanocubes and Their Sensitive Photoluminescence Response toward Hydrogen Peroxide, *ACS Appl. Mater. Interfaces*, 2017, **9**(37), 32097–32105.
16 L. De Trizio, *et al.*, Strongly Fluorescent Quaternary Cu–In–Zn–S Nanocrystals Prepared from $Cu_{1-x}InS_2$ Nanocrystals by Partial Cation Exchange, *Chem. Mater.*, 2012, **24**(12), 2400–2406.
17 P. Ilaiyaraja, *et al.*, Synthesis of Cu-Deficient and Zn-Graded Cu–In–Zn–S Quantum Dots and Hybrid Inorganic-Organic Nanophosphor Composite for White Light Emission, *ACS Appl. Mater. Interfaces*, 2016, **8**(19), 12456–12465.
18 A. Singh, *et al.*, Solution Synthesis and Assembly of Wurtzite-Derived Cu–In–Zn–S Nanorods with Tunable Composition and Band Gap, *Chem. Mater.*, 2015, **27**(5), 1517–1523.
19 A. Zhang, *et al.*, Non-blinking (Zn)CuInS/ZnS Quantum Dots Prepared by In Situ Interfacial Alloying Approach, *Sci. Rep.*, 2015, **5**, 15227.
20 A. Singh, *et al.*, Colloidal synthesis of wurtzite Cu_2ZnSnS_4 nanorods and their perpendicular assembly, *J. Am. Chem. Soc.*, 2012, **134**(6), 2910–2913.
21 A. Singh, *et al.*, Dopant Mediated Assembly of Cu_2ZnSnS_4 Nanorods into Atomically Coupled 2D Sheets in Solution, *Nano Lett.*, 2017, **17**(6), 3421–3428.
22 Y. Zou, X. Su and J. Jiang, Phase-controlled synthesis of Cu_2ZnSnS_4 nanocrystals: the role of reactivity between Zn and S, *J. Am. Chem. Soc.*, 2013, **135**(49), 18377–18384.
23 X. Bai, F. Purcell-Milton and Y. K. Gun'ko, Optical Properties, Synthesis, and Potential Applications of Cu-Based Ternary or Quaternary Anisotropic Quantum Dots, Polytypic Nanocrystals, and Core/Shell Heterostructures, *Nanomaterials*, 2019, **9**(1), 36.
24 X. Bai, F. Purcell-Milton and Y. K. Gun'ko, Near-infrared-emitting CIZSe/CIZS/ZnS colloidal heteronanonail structures, *Nanoscale*, 2020, **12**(28), 15295–15303.

25 S. E. Creutz, *et al.*, Colloidal Nanocrystals of Lead-Free Double-Perovskite (Elpasolite) Semiconductors: Synthesis and Anion Exchange To Access New Materials, *Nano Lett.*, 2018, **18**(2), 1118–1123.
26 Y. Dong, *et al.*, Precise Control of Quantum Confinement in Cesium Lead Halide Perovskite Quantum Dots via Thermodynamic Equilibrium, *Nano Lett.*, 2018, **18**(6), 3716–3722.
27 Z. N. Georgieva, *et al.*, Imprinting Chirality onto the Electronic States of Colloidal Perovskite Nanoplatelets, *Adv. Mater.*, 2018, e1800097.
28 H. Hu, *et al.*, Interfacial Synthesis of Highly Stable $CsPbX_3$/Oxide Janus Nanoparticles, *J. Am. Chem. Soc.*, 2018, **140**(1), 406–412.
29 X. Li, *et al.*, $CsPbX_3$Quantum Dots for Lighting and Displays: Room-Temperature Synthesis, Photoluminescence Superiorities, Underlying Origins and White Light-Emitting Diodes, *Adv. Funct. Mater.*, 2016, **26**(15), 2435–2445.
30 F. Liu, *et al.*, Colloidal Synthesis of Air-Stable Alloyed $CsSn_{1-x}Pb_xI_3$ Perovskite Nanocrystals for Use in Solar Cells, *J. Am. Chem. Soc.*, 2017, **139**(46), 16708–16719.
31 F. Liu, *et al.*, Highly Luminescent Phase-Stable $CsPbI_3$ Perovskite Quantum Dots Achieving Near 100% Absolute Photoluminescence Quantum Yield, *ACS Nano*, 2017, **11**(10), 10373–10383.
32 Z. Liu, *et al.*, Ligand Mediated Transformation of Cesium Lead Bromide Perovskite Nanocrystals to Lead Depleted $Cs_4P_bBr_6$ Nanocrystals, *J. Am. Chem. Soc.*, 2017, **139**(15), 5309–5312.
33 L. Ni, *et al.*, Real-Time Observation of Exciton-Phonon Coupling Dynamics in Self-Assembled Hybrid Perovskite Quantum Wells, *ACS Nano*, 2017, **11**(11), 10834–10843.
34 R. Nie, *et al.*, Mixed Sulfur and Iodide-Based Lead-Free Perovskite Solar Cells, *J. Am. Chem. Soc.*, 2018, **140**(3), 872–875.
35 A. Pan, *et al.*, Nanorod Suprastructures from a Ternary Graphene Oxide-Polymer-$CsPbX_3$ Perovskite Nanocrystal Composite That Display High Environmental Stability, *Nano Lett.*, 2017, **17**(11), 6759–6765.
36 J. Zhang, *et al.*, High Quantum Yield Blue Emission from Lead-Free Inorganic Antimony Halide Perovskite Colloidal Quantum Dots, *ACS Nano*, 2017, **11**(9), 9294–9302.
37 M. J. Cho and S. Y. Park, Preparation of Poly(styrene)-*b*-poly(acrylic acid)-Coupled Carbon Dots and Their Applications, *ACS Appl. Mater. Interfaces*, 2017, **9**(28), 24169–24178.
38 S. Y. Lim, W. Shen and Z. Gao, Carbon quantum dots and their applications, *Chem. Soc. Rev.*, 2015, **44**(1), 362–381.
39 R. Wang, *et al.*, Recent progress in carbon quantum dots: synthesis, properties and applications in photocatalysis, *J. Mater. Chem. A*, 2017, **5**(8), 3717–3734.
40 Y. Wang and A. Hu, Carbon quantum dots: synthesis, properties and applications, *J. Mater. Chem. C*, 2014, **2**(34), 6921–6939.
41 B. Sapkota, *et al.*, Peptide-Decorated Tunable-Fluorescence Graphene Quantum Dots, *ACS Appl. Mater. Interfaces*, 2017, **9**(11), 9378–9387.
42 M. Bacon, S. J. Bradley and T. Nann, Graphene Quantum Dots, *Part. Part. Syst. Charact.*, 2014, **31**(4), 415–428.
43 V. Gupta, *et al.*, Luminscent graphene quantum dots for organic photovoltaic devices, *J. Am. Chem. Soc.*, 2011, **133**(26), 9960–9963.
44 A. Das and P. T. Snee, Synthetic Developments of Nontoxic Quantum Dots, *ChemPhysChem*, 2016, **17**(5), 598–617.
45 K. Dohnalová, *et al.*, Surface brightens up Si quantum dots: direct bandgap-like size-tunable emission, *Light: Sci. Appl.*, 2013, **2**(1), e47–e47.
46 P. M. Fauchet, Light emission from Si quantum dots, *Mater. Today*, 2005, **8**(1), 26–33.
47 W. Zhu, *et al.*, Monodisperse Au nanoparticles for selective electrocatalytic reduction of CO_2 to CO, *J. Am. Chem. Soc.*, 2013, **135**(45), 16833–16836.
48 S. Peng, *et al.*, A facile synthesis of monodisperse Au nanoparticles and their catalysis of CO oxidation, *Nano Res.*, 2008, **1**(3), 229–234.
49 J. Huang, *et al.*, Nanocomposites of size-controlled gold nanoparticles and graphene oxide: formation and applications in SERS and catalysis, *Nanoscale*, 2010, **2**(12), 2733–2738.
50 R. C. Doty, *et al.*, Extremely stable water-soluble Ag nanoparticles, *Chem. Mater.*, 2005, **17**(18), 4630–4635.
51 A. Frattini, *et al.*, Effect of amine groups in the synthesis of Ag nanoparticles using aminosilanes, *Mater. Chem. Phys.*, 2005, **94**(1), 148–152.
52 B. He, *et al.*, Synthesis of size controlled Ag nanoparticles, *J. Mol. Catal. A: Chem.*, 2004, **221**(1–2), 121–126.
53 M. Adam, *et al.*, Colloidal Nanocrystals Embedded in Macrocrystals: Methods and Applications, *J. Phys. Chem. Lett.*, 2016, **7**(20), 4117–4123.
54 S. Kalytchuk, *et al.*, Sodium Chloride Protected CdHgTe Quantum Dot Based Solid-State Near-Infrared Luminophore for Light-Emitting Devices and Luminescence Thermometry, *ACS Photonics*, 2017, **4**(6), 1459–1465.
55 M. Adam, *et al.*, Implementation of High-Quality Warm-White Light-Emitting Diodes by a Model-Experimental Feedback Approach Using Quantum Dot-Salt Mixed Crystals, *ACS Appl. Mater. Interfaces*, 2015, **7**(41), 23364–23371.
56 T. Erdem, *et al.*, Excitonic improvement of colloidal nanocrystals in salt powder matrix for quality lighting and color enrichment, *Opt. Exp.*, 2016, **24**(2), A74–A84.
57 T. Erdem, *et al.*, Stable and efficient colour enrichment powders of nonpolar nanocrystals in LiCl, *Nanoscale*, 2015, **7**(42), 17611–17616.
58 M. Adam, *et al.*, Liquid–Liquid Diffusion-Assisted Crystallization: A Fast and Versatile Approach Toward High Quality Mixed Quantum Dot-Salt Crystals, *Adv. Funct. Mater.*, 2015, **25**(18), 2638–2645.
59 H. Liu, *et al.*, Whispering Gallery Mode Laser from Carbon Dot-NaCl Hybrid Crystals, *ACS Appl. Mater. Interfaces*, 2017, **9**(21), 18248–18253.
60 A. Benad, *et al.*, Cold Flow as Versatile Approach for Stable and Highly Luminescent Quantum Dot-Salt Composites, *ACS Appl. Mater. Interfaces*, 2016, **8**(33), 21570–21575.
61 T. Otto, *et al.*, Colloidal nanocrystals embedded in macrocrystals: robustness, photostability, and color purity, *Nano Lett.*, 2012, **12**(10), 5348–5354.

62 S. Kalytchuk, O. Zhovtiuk and A. L. Rogach, Sodium chloride protected CdTe quantum dot based solid-state luminophores with high color quality and fluorescence efficiency, *Appl. Phys. Lett.*, 2013, **103**(10), 103105.
63 J. F. L. Lox, *et al.*, Brightly Luminescent Cu-Zn-ln-S/ZnS Core/Shell Quantum Dots in Salt Matrices, *Z. Phys. Chem.*, 2019, **233**(1), 23–40.
64 Y. Chang, *et al.*, A water–ethanol phase assisted co-precipitation approach toward high quality quantum dot–inorganic salt composites and their application for WLEDs, *Green Chem.*, 2015, **17**(8), 4439–4445.
65 Y.-M. Huang, *et al.*, The Photothermal Stability Study of Quantum Dots Embedded in Sodium Chlorides, *Crystals*, 2019, **10**(1), 2.
66 M. Müller, *et al.*, Photoluminescence Quantum Yield and Matrix-Induced Luminescence Enhancement of Colloidal Quantum Dots Embedded in Ionic Crystals, *Chem. Mater.*, 2014, **26**(10), 3231–3237.
67 G. Okrepka, Y. Khalavka and Y. Seti, Influence of the KBr matrix on the luminescence properties of CdTe quantum dots, *Luminescence*, 2019, **34**(1), 125–126.
68 T. Erdem, *et al.*, Sweet plasmonics: sucrose macrocrystals of metal nanoparticles, *Nano Res.*, 2014, **8**(3), 860–869.
69 Z. Soran-Erdem, *et al.*, High-Stability, High-Efficiency Organic Monoliths Made of Oligomer Nanoparticles Wrapped in Organic Matrix, *ACS Nano*, 2016, **10**(5), 5333–5339.
70 Z. Soran-Erdem, *et al.*, *Exciton transfer and polarized emission in colloidal quantum dot - anthracene crystals, in 2015 Photonics Conference*. 2015, Ieee: New York.
71 Z. Soran-Erdem, *et al.*, Macrocrystals of Colloidal Quantum Dots in Anthracene: Exciton Transfer and Polarized Emission, *J. Phys. Chem. Lett.*, 2015, **6**(9), 1767–1772.
72 V. Nagarajan, *et al.*, Investigations on the effect of nano Fe_3O_4-doped anthracene single crystal, *Mater. Res. Innovations*, 2017, **22**(1), 13–21.
73 V. Nagarajan, A. Nitthin Ananth and S. Ramaswamy, Investigations onto the role of transition metal oxide dopants in anthracene crystals, *Mater. Res. Exp.*, 2017, **4**(12), 125102.
74 X. Shen, *et al.*, Efficient and Stable $CsPb(Br/I)_3$@Anthracene Composites for White Light-Emitting Devices, *ACS Appl. Mater. Interfaces*, 2018, **10**(19), 16768–16775.
75 H. El-Swie, *et al.*, Fluorescence, thermal and mechanical properties of PMMA-CdSe QD film, *J. Optoelectron. Adv. Mater.*, 2017, **19**(3–4), 228–233.
76 D. Sun, N. Miyatake and H.-J. Sue, Transparent PMMA/ZnO nanocomposite films based on colloidal ZnO quantum dots, *Nanotechnology*, 2007, **18**(21), 215606.
77 I. Suarez, *et al.*, Photoluminescence waveguiding in CdSe and CdTe QDs-PMMA nanocomposite films, *Nanotechnology*, 2011, **22**(43), 435202.
78 M. Zhang, *et al.*, Preparation of all-inorganic perovskite quantum dots-polymer composite for white LEDs application, *J. Alloys Compd.*, 2018, **748**, 537–545.
79 L. Protesescu, *et al.*, Nanocrystals of Cesium Lead Halide Perovskites (CsPbX(3), X = Cl, Br, and I): Novel Optoelectronic Materials Showing Bright Emission with Wide Color Gamut, *Nano Lett.*, 2015, **15**(6), 3692–3696.
80 J. Xu and D. Li, Preparation and Photoluminescence of Transparent Poly(methyl methacrylate)-Based Nanocomposite Films with Ultra-High-Loading Pendant ZnS Quantum Dots, *Polymers*, 2018, **10**(11), 1217.
81 L. Pang, *et al.*, PMMA quantum dots composites fabricated via use of pre-polymerization, *Opt. Exp.*, 2005, **13**(1), 44–49.
82 Y. Ma, *et al.*, Bulk synthesis of homogeneous and transparent bulk core/multishell quantum dots/PMMA nanocomposites with bright luminescence, *J. Appl. Polym. Sci.*, 2013, **130**(3), 1548–1553.
83 F. Meinardi, *et al.*, Large-area luminescent solar concentrators based on 'Stokes shift-engineered' nanocrystals in a mass-polymerized PMMA matrix, *Nat. Photonics*, 2014, **8**(5), 392–399.
84 S. Li, *et al.*, Bulk Synthesis of Transparent and Homogeneous Polymeric Hybrid Materials with ZnO Quantum Dots and PMMA, *Adv. Mater.*, 2007, **19**(24), 4347–4352.
85 C. Li, *et al.*, Large Stokes Shift and High Efficiency Luminescent Solar Concentrator Incorporated with $CuInS_2$/ZnS Quantum Dots, *Sci. Rep.*, 2015, **5**, 17777.
86 G. Landi, *et al.*, Investigation of the optical characteristics of a combination of InP/ZnS-quantum dots with MWCNTs in a PMMA matrix, *Opt. Mater.*, 2013, **35**(12), 2490–2495.
87 C. Kok Sheng, Investigation of Morphological, Structural and Electrical Properties of Cds/ PMMA Nanocomposite Film Prepared by Solution Casting Method, *Int. J. Electrochem. Sci.*, 2017, 10023–10031.
88 I. V. Kityk, *et al.*, Drastic increase in the second-order optical susceptibilities for monodisperse In2O3nanocrystals incorporated into PMMA matrices, *Nanotechnology*, 2006, **17**(8), 1871–1877.
89 P. K. Khanna and N. Singh, Light emitting CdS quantum dots in PMMA: synthesis and optical studies, *J. Lumin.*, 2007, **127**(2), 474–482.
90 Y. Huang, *et al.*, Preparation and multicolored fluorescent properties of CdTe quantum dots/polymethylmethacrylate composite films, *J. Alloys Compd.*, 2015, **647**, 578–584.
91 S. K. E. Hill, *et al.*, Silicon Quantum Dot–Poly(methyl methacrylate) Nanocomposites with Reduced Light Scattering for Luminescent Solar Concentrators, *ACS Photonics*, 2018, **6**(1), 170–180.
92 S. K. E. Hill, *et al.*, Poly(methyl methacrylate) Films with High Concentrations of Silicon Quantum Dots for Visibly Transparent Luminescent Solar Concentrators, *ACS Appl. Mater. Interfaces*, 2020, **12**(4), 4572–4578.
93 H. Gordillo, *et al.*, Color Tuning and White Light by Dispersing CdSe, CdTe, and CdS in PMMA Nanocomposite Waveguides, *IEEE Photonics J.*, 2013, **5**(2), 2201412.
94 H. Gordillo, *et al.*, Polymer/QDs Nanocomposites for Waveguiding Applications, *J. Nanomater.*, 2012, **2012**, 1–9.
95 S. M. El-Bashir, *et al.*, Red photoluminescent PMMA nanohybrid films for modifying the spectral distribution of solar radiation inside greenhouses, *Renewable Energy*, 2016, **85**, 928–938.

96 D. Patidar, S. Agrawal and N. S. Saxena, Storage modulus and glass transition behaviour of CdS/PMMA nanocomposites, *J. Exp. Nanosci.*, 2011, **6**(4), 441–449.
97 I. Moura, *et al.*, Morphology, optical, and electric properties of polymer-quantum dots nanocomposites: effect of polymeric matrix, *J. Mater. Sci.*, 2016, **51**(18), 8699–8710.
98 A. Marinins, *et al.*, Light-Converting Polymer/Si Nanocrystal Composites with Stable 60–70% Quantum Efficiency and Their Glass Laminates, *ACS Appl. Mater. Interfaces*, 2017, **9**(36), 30267–30272.
99 M. J. Smith, *et al.*, Robust, Uniform, and Highly Emissive Quantum Dot-Polymer Films and Patterns Using Thiol–Ene Chemistry, *ACS Appl. Mater. Interfaces*, 2017, **9**(20), 17435–17448.
100 M. H. Stewart, *et al.*, Fabrication of Photoluminescent Quantum Dot Thiol–yne Nanocomposites via Thermal Curing or Photopolymerization, *ACS Omega*, 2018, **3**(3), 3314–3320.
101 D. A. Boyd, *et al.*, Small-molecule detection in thiol–yne nanocomposites via surface-enhanced Raman spectroscopy, *Anal. Chem.*, 2014, **86**(24), 12315–12320.
102 J. P. Phillips, *et al.*, Dispersion of Gold Nanoparticles in UV-Cured, Thiol–Ene Films by Precomplexation of Gold–Thiol, *Chem. Mater.*, 2008, **20**(16), 5240–5245.
103 C.-H. Kim, *et al.*, Fabrication of highly photoluminescent quantum dot-polymer composite micropatterned surface using thiol–ene chemistry, *RSC Adv.*, 2016, **6**(99), 96700–96705.
104 F. Meinardi, *et al.*, Highly efficient large-area colourless luminescent solar concentrators using heavy-metal-free colloidal quantum dots, *Nat. Nanotechnol.*, 2015, **10**(10), 878–885.
105 D. I. Shiman, *et al.*, Robust Polymer Matrix Based on Isobutylene (Co)polymers for Efficient Encapsulation of Colloidal Semiconductor Nanocrystals, *ACS Appl. Nano Mater.*, 2019, **2**(2), 956–963.
106 G. Wang, *et al.*, Tunable effective nonlinear refractive index of graphene dispersions during the distortion of spatial self-phase modulation, *Appl. Phys. Lett.*, 2014, **104**(14), 141909.
107 G. Wang, *et al.*, Tunable nonlinear refractive index of two-dimensional MoS_2, WS_2, and $MoSe_2$ nanosheet dispersions, *Photonics Res.*, 2015, **3**(2), A51–A55.
108 G. Wang, *et al.*, Ultrafast Carrier Dynamics and Bandgap Renormalization in Layered $PtSe_2$, *Small*, 2019, **15**(34), 1902728.
109 G.-K. Lim, *et al.*, Giant broadband nonlinear optical absorption response in dispersed graphene single sheets, *Nat. Photonics*, 2011, **5**(9), 554–560.
110 G. Wang, *et al.*, Broadband saturable absorption and exciton–exciton annihilation in $MoSe_2$ composite thin films, *Opt. Mater. Exp.*, 2019, **9**(2), 483–496.
111 G. Wang, *et al.*, Nonlinear optical performance of few-layer molybdenum diselenide as a slow-saturable absorber, *Photonics Res.*, 2018, **6**(7), 674–680.
112 G. Wang, A. A. Baker-Murray and W. J. Blau, Saturable Absorption in 2D Nanomaterials and Related Photonic Devices, *Laser Photonics Rev.*, 2019, **13**(7), 1800282.
113 A. C. Tam and C. K. N. Patel, Two-photon absorption spectra and cross-section measurements in liquids, *Nature*, 1979, **280**(5720), 304–306.
114 L.-F. Gao, *et al.*, Small molecule-assisted fabrication of black phosphorus quantum dots with a broadband nonlinear optical response, *Nanoscale*, 2016, **8**(33), 15132–15136.
115 Y. Xu, *et al.*, Stabilization of black phosphorous quantum dots in PMMA nanofiber film and broadband nonlinear optics and ultrafast photonics application, *Adv. Funct. Mater.*, 2017, **27**(32), 1702437.
116 M. B. H. Mahyuddin, *et al.*, Quantum dot cadmium selenide as a saturable absorber for Q-switched and mode-locked double-clad ytterbium-doped fiber lasers, *Opt. Commun.*, 2017, **397**, 147–152.
117 W. Chung, *et al.*, White emission using mixtures of CdSe quantum dots and PMMA as a phosphor, *Opt. Mater.*, 2010, **32**(4), 515–521.
118 X. Dai, *et al.*, Solution-processed, high-performance light-emitting diodes based on quantum dots, *Nature*, 2014, **515**(7525), 96–99.
119 M. Rahmati, *et al.*, Highly Efficient Quantum Dot Light-Emitting Diodes by Inserting Multiple Poly(methyl methacrylate) as Electron-Blocking Layers, *Adv. Funct. Mater.*, 2019, **29**(50), 1906742.
120 H. Li, *et al.*, Doctor-blade deposition of quantum dots onto standard window glass for low-loss large-area luminescent solar concentrators, *Nat. Energy*, 2016, **1**(12), 16157.
121 F. Li, *et al.*, Highly Stable and Spectrally Tunable Gamma Phase $Rb_xCs_{1-x}PbI_3$ Gradient-Alloyed Quantum Dots in PMMA Matrix through A Sites Engineering, *Adv. Funct. Mater.*, 2021, **31**(11), 2008211.
122 C. Maoquan and L. Guojie, Fluorescent Silkworm Silk Prepared via Incorporation of Green, Yellow, Red, and Near-Infrared Fluorescent Quantum Dots, *IEEE Trans. Nanotechnol.*, 2008, **7**(3), 308–315.
123 J. B. van Beilen and Y. Poirier, Establishment of new crops for the production of natural rubber, *Trends Biotechnol.*, 2007, **25**(11), 522–529.
124 C. N. Rochette, *et al.*, Shell structure of natural rubber particles: evidence of chemical stratification by electrokinetics and cryo-TEM, *Langmuir*, 2013, **29**(47), 14655–14665.
125 C. S. Danna, *et al.*, Flexible fluorescent films based on quantum dots (QDs) and natural rubber, *J. Appl. Polym. Sci.*, 2017, **134**(43), 45459.
126 J. Huang, Q. Li and Z. Shao, Fabricating highly luminescent solid hybrids based on silicon nanoparticles: a simple, versatile and green method, *Nanoscale*, 2018, **10**(21), 10250–10255.
127 H. Tetsuka, T. Ebina and F. Mizukami, Highly Luminescent Flexible Quantum Dot-Clay Films, *Adv. Mater.*, 2008, **20**(16), 3039–3043.
128 C.-H. Zhou, *et al.*, Preparation and functionality of clay-containing films, *J. Mater. Chem.*, 2011, **21**(39), 15132–15153.
129 M. Xia, *et al.*, Semiconductor quantum dots-embedded inorganic glasses: fabrication, luminescent properties, and potential applications, *Adv. Opt. Mater.*, 2019, **7**(21), 1900851.

130 M. He, *et al.*, Doping manganese into $CsPb(Cl/Br)_3$ quantum dots glasses: dual-color emission and super thermal stability, *J. Am. Ceram. Soc.*, 2019, **102**(3), 1090–1100.
131 K. Xu and J. Heo, Effect of Silver Ion-exchange on the precipitation of lead sulfide quantum dots in glasses, *J. Am. Ceram. Soc.*, 2012, **95**(9), 2880–2884.
132 K. Xu and J. Heo, Luminescence enhancement of CdS quantum dots in glass by Ag^+ ion exchange, *J. Am. Ceram. Soc.*, 2013, **96**(4), 1138–1142.
133 H. Minti, *et al.*, Quantum dots of cadmium sulfide in thin glass films prepared by sol–gel technique, *Chem. Phys. Lett.*, 1991, **183**(3-4), 277–282.
134 T. Takada, *et al.*, Preparation and non-linear optical properties of CdS quantum dots in Na_2O–B_2O_3–SiO_2 glasses by the sol–gel technique, *J. Mater. Sci.*, 1996, **31**(2), 423–430.
135 E. Cattaruzza, Quantum-dot composite silicate glasses obtained by ion implantation, *Nucl. Instrum. Methods Phys. Res., Sect. B*, 2000, **169**(1–4), 141–155.
136 R. Haglund Jr, *et al.*, Nonlinear optical properties of metal-quantum-dot composites synthesized by ion implantation, *Nucl. Instrum. Methods Phys. Res., Sect. B*, 1994, **91**(1-4), 493–504.
137 S. Munishwar, *et al.*, Highly stable CdS quantum dots embedded in glasses and its application for inhibition of bacterial colonies, *Opt. Mater.*, 2020, **99**, 109590.
138 C. H. Ravikumar, R. Shwetharani and R. G. Balakrishna, Surface modified glass substrate for sensing *E. coli* using highly stable and luminescent CdSe/CdS core shell quantum dots, *J. Photochem. Photobiol., B*, 2020, **204**, 111799.
139 J. Lin, *et al.*, Perovskite quantum dots glasses based backlit displays, *ACS Energy Lett.*, 2021, **6**(2), 519–528.
140 B. Zhuang, *et al.*, Glass stabilized ultra-stable dual-emitting Mn-doped cesium lead halide perovskite quantum dots for cryogenic temperature sensing, *Nanoscale*, 2019, **11**(32), 15010–15016.
141 K. Han, S. Yoon and W. J. Chung, CdS and CdSe quantum dot-embedded silicate glasses for LED color converter, *Int. J. Appl. Glass Sci.*, 2015, **6**(2), 103–108.
142 Q. Yang, *et al.*, UV-shielding device of high-stability glass embedded with in-situ growth of ZnO quantum dots, *J. Alloys Compd.*, 2019, **784**, 535–540.
143 Z. Hu, *et al.*, Co-doping of Ag into Mn:ZnSe Quantum Dots: Giving Optical Filtering effect with Improved Monochromaticity, *Sci. Rep.*, 2015, **5**(1), 14817.
144 S. Reda, Synthesis and optical properties of CdS quantum dots embedded in silica matrix thin films and their applications as luminescent solar concentrators, *Acta Mater.*, 2008, **56**(2), 259–264.
145 X. Wan, *et al.*, The third order optical nonlinear character of ZnSe nanocrystals doped silica glasses, *J. Electroceram.*, 2008, **21**(1), 737–740.
146 N. Thantu, Second harmonic generation and two-photon luminescence upconversion in glasses doped with ZnSe nanocrystalline quantum dots, *J. Lumin.*, 2005, **111**(1–2), 17–24.
147 G. Mandal, *et al.*, Cadmium-free quantum dots as time-gated bioimaging probes in highly-autofluorescent human breast cancer cells, *Chem. Commun.*, 2013, **49**(6), 624–626.
148 S. J. Lim, A. Smith and S. Nie, The More Exotic Shapes of Semiconductor Nanocrystals: Emerging Applications in Bioimaging, *Curr. Opin. Chem. Eng.*, 2014, **4**, 137–143.
149 F. Purcell-Milton and Y. K. Gun'ko, Quantum dots for Luminescent Solar Concentrators, *J. Mater. Chem.*, 2012, **22**(33), 16687–16697.